VirtualBrainCloud

Personalized Recommendations for Neurodegenerative Disease

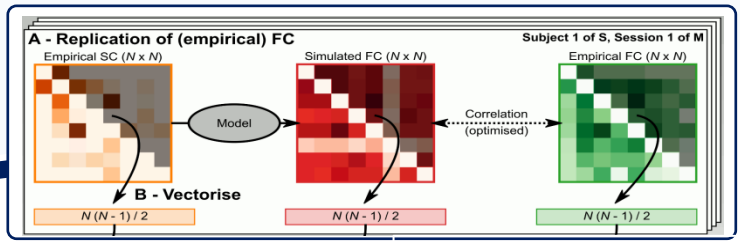

www.VirtualBrainCloud-2020.eu

Public deliverable report

D3.11: Multi-resolution TVB models with evidence for optimal granularity

Date	May 2023
Authors	Institute of Neuroscience and Medicine (INM-7; Brain and Behaviour) Forschungszentrum Oleksandr V. Popovych, Justin W.M. Domhof, Simon B. Eickhoff

Dissemination level	**public**
Website	www.VirtualBrainCloud-2020.eu

This project has received funding from the **European Union´s Horizon 2020** research and innovation programme under **grant agreement No 826421**

Table of content

Background

The current deliverable is developed in the framework of the VirtualBrainCloud project that is dedicated to investigation and application of the brain modeling, big data and high-performance computing to personalized prevention and treatment of neurodegenerative diseases. Here, the personalized brain modeling by dynamical whole-brain models plays an important role, which can bridge a gap between the brain structure and function with a great potential for mechanistic explanations of brain dynamics and function and hypothesis testing *in cilico*. The data-driven modeling approaches are in active development nowadays, where the empirical neuroimaging data are used for the model derivation and validation. Following the main ideas in the brain research representing the brain as a collection of networks of functional units, the network-based dynamical models essentially involve brain atlases that relay on *a priori* knowledge on the brain organization and function. They parcel the brain into separate regions according to dedicated algorithms with different levels of granularity, which serve as a backbone for the model networks. However, little is known about the impact of brain parcellations on the empirical data used for the modeling and on the modeling outcomes. This deliverable aims at investigation of the effect of brain parcellations and their granularity in particular on the properties of empirical and simulated connectomes, validation quality of the whole-brain dynamical models and reliability and specificity of the modeling results.

1. Introduction

The widely-used connectivity-based approaches to investigate the complex brain structure and function suggest to represent the brain as a collection of structural or functional networks, where nodes encapsulate brain regions while edges consolidate the structural or functional connectivity among these regions, respectively (Park and Friston, 2013; Schaefer *et al.*, 2018; Messe, 2019; Zimmermann *et al.*, 2019; Pervaiz *et al.*, 2020). Brain regions can be delimited using a parcellation, i.e., brain atlases whose properties are in the focus of the contemporary brain research (Eickhoff, Yeo and Genon, 2018). However, the great variety of possible techniques for brain parcellation and existing brain atlases makes the choice of a particular parcellation very difficult, and there is no consensus on which brain atlas is more adequate for a given analysis (Thirion *et al.*, 2014; Eickhoff, Constable and Yeo, 2018; Eickhoff, Yeo and Genon, 2018). The choice of an appropriate brain parcellation is one of the main issues also for the modeling of the resting-state brain dynamics by whole-brain dynamical models (Ghosh *et al.*, 2008; Honey *et al.*, 2009; Popovych *et al.*, 2019). Indeed, the derivation and validation of the models essentially utilize the empirical structural and functional connectomes, whose calculations in turn are based on a given parcellation of the brain into separate regions.

Several studies addressed the properties of the brain parcellations with application to empirical neuroimaging data. For example, a few clustering approaches were applied to the task-based functional magnetic resonance imaging (fMRI) data and compared with respect to their accuracy and reproducibility (Thirion *et al.*, 2014). It was in particular found that the reproducibility can peak at about ~200 clusters, whereas the accuracy seemed to monotonically increase up to ~5000 clusters. The two criteria thus diverge imposing a trade-off choice between accuracy and stability. A systematic comparison between many anatomical, connectivity-driven and random parcellation methods was also conducted with application to the resting-state functional connectivity (FC) of fMRI data according to a few criteria including reproducibility, fidelity, agreement with fMRI task activation, myelin maps, and

cytoarchitectural areas, and network analysis (Arslan *et al.*, 2018). The study did not found any optimal parcellation method capable to address all the challenges simultaneously, where the most of the evaluated measures monotonically vary with respect to the number of parcels. However, the considered network measures like clustering coefficient, characteristic path length and the average node degree exhibit some optimality at the granularity of about ~150-200 parcels, but not the small-world index (Arslan *et al.*, 2018). In contrast, the network properties of the structural connectivity (SC) calculated by the whole-brain tractography (WBT) from the diffusion-weighted MRI (dwMRI) again manifested a monotonic dynamics with respect to the parcellation granularity (Zalesky *et al.*, 2010). Other recent studies have reported empirical evidence for the effects of atlas selection on subject specificity, structure-function relationship and data-driven prediction of behavioral traits (Messe, 2019; Zimmermann *et al.*, 2019; Pervaiz *et al.*, 2020). In particular, the structure-function relationship between SC and the resting-state FC was shown to exhibit a monotonic decay as the number of regions in the considered state-of-the-art brain atlases increased.

As follows, already for the empirical neuroimaging data and empirical connectomes there is no general consensus as to which parcellation and which granularity would be most appropriate for a given analysis. The situation is more involved for the data-informed whole-brain models, where the empirical SC and FC are used for the model derivation and validation. The models thus inherit all problems of the empirical data in addition to the complicated procedures of model validation and parameter optimization. Only a few studies addressed this question. The influence of parcellation granularity and local connectivity on slow and fast dynamics of coupled neuronal mass models was investigated in paper (Proix *et al.*, 2016) for a random splitting of the Desikan-Killiany atlas (Desikan *et al.*, 2006) into smaller subregions. The data processing parameter of the number of streamlines in the WBT was shown to be important for the quality of the model fitting, which was affected by selected brain parcellation (Jung, Eickhoff and Popovych, 2021). The inter-subject and inter-parcellation variability of the goodness-of-fit (GoF) values of the model to the empirical data was investigated for 11 and for 19 state-of-the-art parcellations in our recent papers (Popovych *et al.*, 2021) and (Domhof *et al.*, 2021), respectively. It was in particular shown that the statistical data indices and the graph-theoretical network properties of empirical connectomes can well account for the inter-parcellation variability of the modeling results. However, only the former can also well explain the inter-subject model variability, which strongly depends on the selected brain parcellation. Given such an enhanced model variability, we also investigated the test-retest reliability and subject specificity of the modeling results and showed that the simulated FC can outperform the empirical FC in terms of both reliability and subject specificity, which again depends on the considered brain parcellation (Domhof, Eickhoff and Popovych, 2022b). An appropriate selection of the brain parcellation is also crucial for improved classification of the patients with Parkinson's disease from the healthy subjects with involvement of the whole-brain dynamical models (Jung *et al.*, 2022).

In the current deliverable we illustrate the impact of the brain parcellations on the empirical data and modeling results. We initiated such an investigation in the previous deliverable D3.09 "Evaluation of cross-model atlas-based compression for machine learning" (Domhof *et al.*, 2020) and enhanced it in the next deliverable D3.10 "Framework for multi-modal integrated annotations established and in use" (Popovych and Eickhoff, 2021). In the current report we focus more on the impact of the parcellation granularity on the neuroimaging data used for the modeling as well as on the modeling results. We show that the parcellation granularity can contribute to the variability of the averaged GoF values of the model across different parcellations. However this factor can only partially explain the inter-parcellation

heterogeneity of the empirical data and the modeling results, and the observed parcellation-induced deviations typically go beyond a simple relationship with the number of parcels. The variability in the modeling results as reflected by their GoF values, reliability and subject specificity is still large across parcellations with similar granularity, which indicates that other parcellation properties like modality of the neuroimaging data (structural/functional) and algorithms employed for the parcellation must be taken into account for a better explanation of the impact of brain parcellation of the empirical and simulated data.

2. Partners involved

This deliverable was prepared by the Institute of Neuroscience and Medicine (Brain and Behaviour, INM-7) from the Forschungszentrum Jülich (FZJ). The computational resources were granted through JARA on the supercomputer JURECA (Jülich Supercomputing Centre, 2021) at Jülich Supercomputing Centre, Forschungszentrum Jülich.

3. Description of work performed

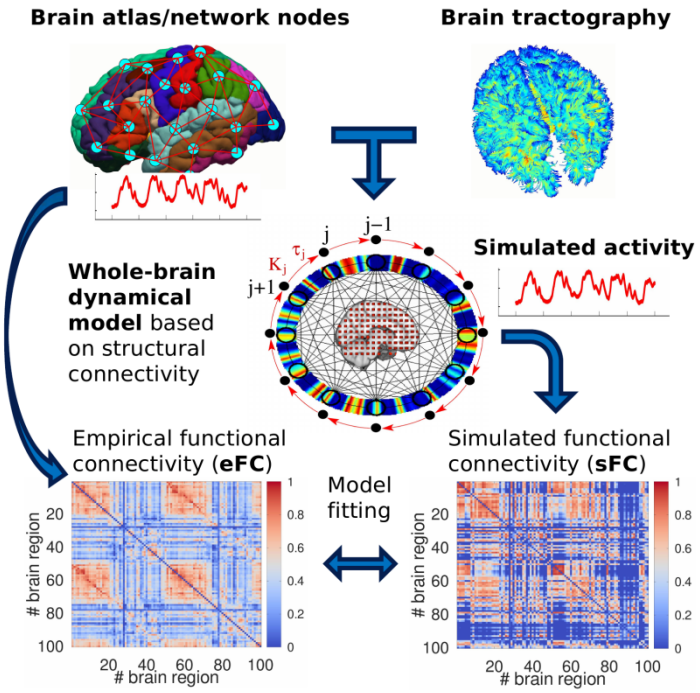

Figure 1. Derivation and validation of a whole-brain dynamical model. First, brain regions parcellated according to a given brain atlas serve as nodes in the model network (upper left), where the inter-node connections are extracted from the empirical SC calculated from the WBT and dwMRI data (upper right). Second, the empirical FC (eFC) of the atlas-based network of regions is computed via correlating the resting-state mean blood oxygen level-dependent (BOLD) signals of any two parcels (lower left). Third, simulated FC (sFC) is calculated via correlating the simulated BOLD time series generated for each network node by the derived model (lower right). Finally, the model parameters are optimized by model fitting to empirical data in such a way that the sFC approximates the eFC as closely as possible.

The derivation and validation of the whole-brain dynamical models is schematically depicted in Figure 1. Brain parcellation is used to split the brain into separate regions that define the nodes of a model network (Ghosh *et al.*, 2008; Honey *et al.*, 2009; Popovych *et al.*, 2019). The inter-nodes connections

are derived from the empirical SC (matrices of streamline counts and averaged streamline pathlength) calculated according to a given parcellation by the WBT from dwMRI, which constitutes a so-called brain structural connectome (Sporns, Tononi and Kotter, 2005). Each node of the model network is equipped by local dynamics that is governed by a dynamical system modeling in such a way the averaged (neuronal) activity of the respective brain region. We considered several brain parcellations based on the structural and functional brain properties and several dynamical models for the local dynamics including phase and limit-cycle oscillators, Wilson-Cowan neural mass model and reduced Jansen-Rit model, see Refs. (Domhof *et al.*, 2021; Jung, Eickhoff and Popovych, 2021; Popovych *et al.*, 2021; Domhof, Eickhoff and Popovych, 2022b; Jung *et al.*, 2022) for model details. The considered model was used to generate simulated blood oxygen level-dependent (BOLD) signals that were used to calculate other derivatives, for example, simulated FC by pairwise correlations of the BOLD signals of any two oscillators in the ensemble modeling the dynamics of the parcellated regions in the brain. The model was validated by comparing the simulated and empirical data, where the model parameters were optimized in order to obtain the closest correspondence between the model output and the respective empirical counterpart. For example, the correlation between simulated and the resting-state empirical FCs can be maximized by optimization of the model parameters and considered as a goodness-of-fit (GoF) of the model to empirical data for further analyses together with the optimal model parameters.

3.1. Inter-parcellation and inter-individual variability

In this deliverable we first illustrate how the parcellations may impact the distribution of GoF values for individual subjects. We compared these distributions between 11 different parcellations of different granularities of three brain atlases as given by the Schaefer atlas (Schaefer *et al.*, 2018), the Harvard-Oxford atlas (Desikan *et al.*, 2006) and the Shen atlas (Shen *et al.*, 2013). Several parcellations of these atlases were considered: the Schaefer atlas with 100, 200, 400 and 600 cortical parcels (denoted as S100, S200, S400 and S600, respectively), the Shen atlas with 79, 156 and 232 cortical regions (denoted as Shen79, Shen156 and Shen232), and the probabilistic Harvard-Oxford atlas with 96 non-overlapping cortical parcels with thresholds at 0%, 25%, 35%, and 45% of the maximal probability (denoted as HO96 0%, HO96 25%, HO96 35%, and HO96 45%, respectively). For the higher thresholding, voxels that did not reach the threshold level were excluded, which makes the parcellated brain regions smaller as the threshold increases.

To evaluate the impact of brain parcellations on the statistical properties of the resting-state brain dynamics and connectivity, several data indices (or data variables) were calculated from the empirical data used for the model derivation and validation. For example, the standard deviation (denoted here as '*std*') of time fluctuations of BOLD signals was calculated first and then averaged (denoted here as '*aver*') over all parcels. The obtained data variable denoted as *aver*[*std*(BOLD)] is an average extent of BOLD fluctuation for a given subject. The operations of '*std*' and '*aver*' can be applied in different combinations to the empirical FC and SC. For example, the extent of total averaged functional connectivity (average synchronization between any two regions) in the brain is *aver*[*aver*(eFC)] or it's inter-regional variability is *std*[*aver*(eFC)]. Such an approach was also applied to the structural connectomes (streamline counts – eSC and averaged streamline pathlength – ePL), see Ref. (Popovych *et al.*, 2021) for details. Also the structure-function relationship *corr*(eFC, eSC) between empirical functional and structural connectivities was evaluated by Pearson correlation involving ePL as well.

The GoF values were then compared with the statistical data indices calculated from the empirical data in order to explain where the inter-subject and inter-parcellation variability of the modeling results may come from. The results were obtained for two models of the local dynamics based on the phase and limit-cycle oscillators that directly modeled the ultra-slow oscillations of the resting-state BOLD signals.

Table 1: Overview of the used brain parcellation schemes with the index for reference in this study, the number of parcels (#parcels) and associated publications. Colors are used to highlight the parcellations in Figure 5.

Index	Name	#parcels	Refs. (see (Domhof *et al.*, 2021) for more details)
1	MIST	31	(Urchs et al., 2019)
2		56	
3		103	
4		167	
5	Craddock	38	(Craddock et al., 2012)
6		56	
7		108	
8		160	
9	Shen 2013	79	(Shen et al., 2013)
10		156	
11	Schaefer (17 networks)	100	(Schaefer et al., 2018)
12		200	
13	Harvard-Oxford	48	(Desikan et al., 2006; Frazier et al., 2005; Goldstein et al., 2007; Makris et al., 2006)
14		96	
15	Desikan-Killiany	70	(Desikan et al., 2006)
16	von Economo-Koskinas	86	(Scholtens et al., 2018; von Economo and Koskinas, 1925)
17	AAL (version 2)	92	(Rolls et al., 2015; Tzourio-Mazoyer et al., 2002)
18	Destrieux	150	(Destrieux et al., 2010)
19	Brainnetome	210	(Fan et al., 2016)

The obtained results were generalized for 19 parcellations (Table 1), for the phase oscillators and Wilson-Cowan model, and for the graph-theoretical network properties served as data indices to account for the inter-parcellation and inter-individual variability of the empirical data and modeling results. We thus extracted some network metrics from the empirical SC and PL and the empirical and simulated FC matrices. To be specific, we determined the *degree distribution* and the *modularity* of the empirical SC and both types of FC to characterize their centrality and segregation, respectively. In addition, we calculated the *closeness centrality* distribution and the *global efficiency* of the ePL matrix as representations of its centrality and integration, respectively. Furthermore, we calculated the *clustering coefficients* from the empirical SC and FC and the *characteristic path lengths* from the empirical PL and FC matrices, see Refs. (Rubinov and Sporns, 2010; Domhof *et al.*, 2021) for details.

3.2. Reliability and subject specificity

To study the inter- and intra-subject variability of the modeling results in more detail we investigated the impact of brain parcellation on the test-retest reliability and subject specificity of the modeling results and their relation to empirical data. We used the empirical connectomes of the previous study that have already been published elsewhere (Domhof *et al.*, 2022b). In particular, we used the empirical SC and FC matrices of $S = 200$ subjects from the Human Connectome Project (HCP) S1200 release dataset (Van Essen *et al.*, 2013) that were reconstructed on the basis of 8 different parcellations from Table 1 with the indices 3 (MIST), 7 (CD), 9 (Shen), 11 (Sch.), 14 (HO), 15 (DK), 16 (EK), and 17 (AAL). Here, each parcellation has a similar number of *N* brain regions, and each subject has *M* = 4 different

empirical FCs that correspond to the 4 separate resting-state fMRI sessions included in the original (HCP) dataset for each subject.

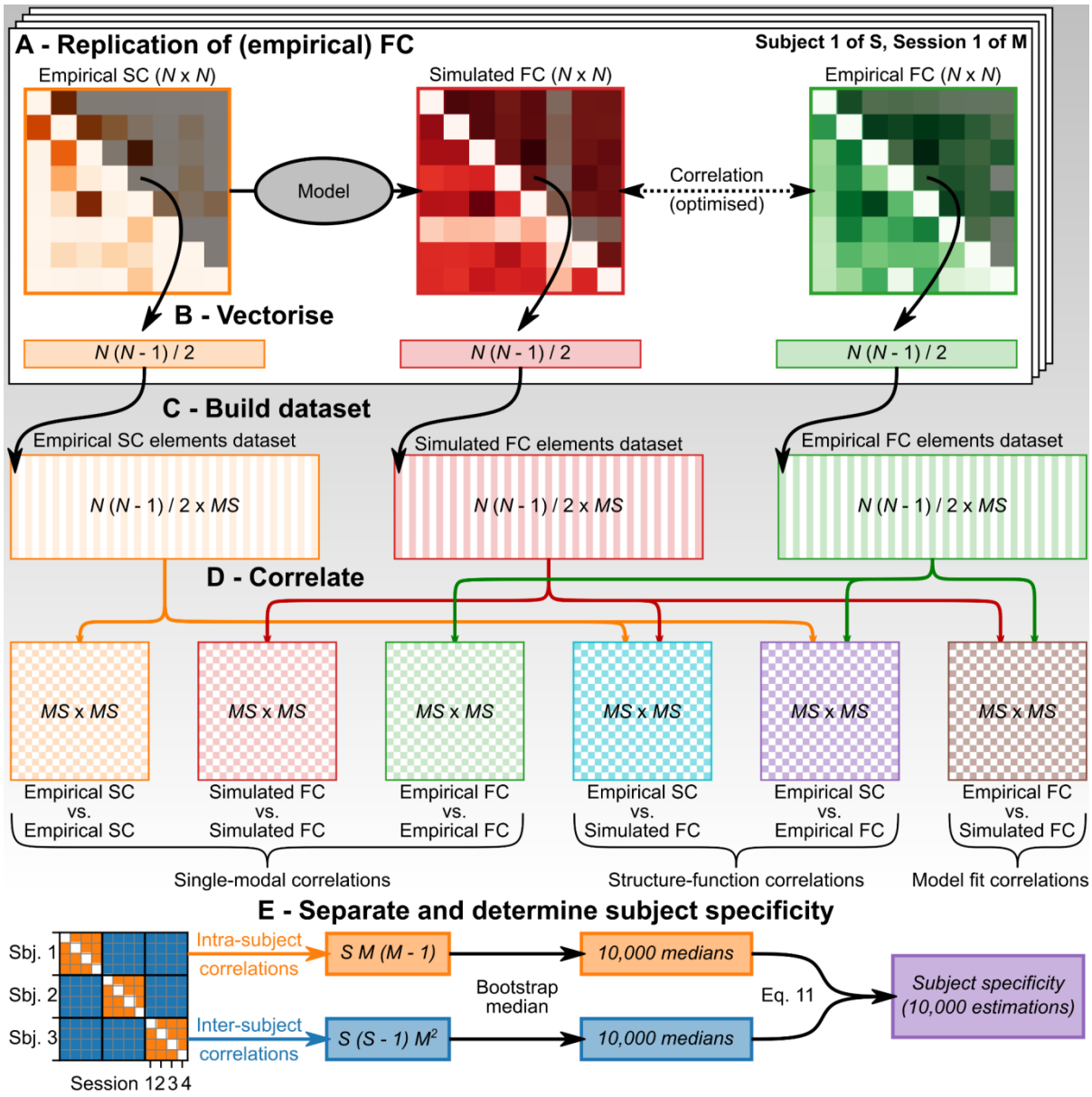

Figure 2. Schematic illustration of the methodology used to evaluate the test-retest reliability and subject specificity of the empirical and simulated connectomes. (A) Dynamical whole-brain models were used to sample the simulated FC matrices that replicated the empirical FC as well as possible. (B) The upper triangles of the empirical SC, empirical FC and simulated FC matrices of dimension *N x N* were vectorized to vectors of *N(N-1)/2* elements. (C) These vectors were gathered into datasets of *MS* vector columns that contained the individual connectomes of all *S* subjects and their *M* separate fMRI sessions. (D) The connectome datasets were (cross-)correlated, where the obtained cross-correlation matrices of dimension *MS x MS* were used to quantify the inter- and intra-subject similarities/differences between individual connectomes. (E) The cross-correlation matrix is illustrated here for 3 subjects (sbj.) (*S = 3, M = 4*), where the inter- and intra-subject correlations (blue and orange matrix elements, respectively) were collected in separate vectors. Their medians were bootstrapped 10,000 times.

We investigated the inter- and intra-subject variations of the empirical SC, the empirical FC, the simulated FC and their single- and bi-modal relationships (correlations). To do so, we vectorized the off-diagonal upper triangles of the connectivity matrices (Figure 2A-B), and gathered the resulting vectors

of all *S* subjects in one dataset separately for each type of connectivity and parcellation (Figure 2C). Here, as there was only one realization of the empirical SC available, we repeated the vectors of the empirical SC matrix *M* times (*M* being the number of resting-state fMRI sessions per subject) to match the dimensions of the datasets of the other connectivity types. Subsequently, we calculated the Pearson correlation coefficients across the individual connections between these datasets. The result comprised a number of *MS* x *MS* (cross-)correlation matrices that correspond to either one of three types of correlations: single-modal correlations, structure-function correlations and model fit correlations (Figure 2D). The *single-modal correlations* are the correlations between the same type of connectivity (e.g. empirical FC vs. empirical FC). They characterize the reproducibility of the connectivity matrices. The *structure-function* correlations are the cross-correlations of the empirical SC with the empirical FC or the simulated FC, and the *model fit correlations* comprise the correlations between the empirical and the simulated FC. The latter two types of correlations quantify the extent to which the different types of connectivity have mutual patterns.

The within-subject, single-modal correlations characterize whether model fits are realized through converging connectivity patterns of simulated FC. However, these patterns may be more similar in general, that is, also across different subjects. We therefore calculated the specificity index *Specificity*, where the mean between-subject correlation $Corr_{between}$ was subtracted from the mean within-subject correlation $Corr_{within}$: $Specificity = Corr_{within} - Corr_{between}$, which is similar to the approach of Refs. (Amico and Goni, 2018; Zimmermann *et al.*, 2019). The specificity index reflects whether connectomes are indeed reproduced better (more similar to each other) within than between subjects and can be used to quantify the subject specificity. To assess the variations in the subject specificity (or the differences between the median inter- and intra-subject correlations), we bootstraped the median correlations many times (Figure 2E). The subject-specificity index (correlation difference) is then calculated for each bootstrap so that its 95% confidence interval can be constructed, which in turn reveals whether the observed differences are significant.

We also used the intraclass correlation (ICC) to characterize the reliability of the simulation results obtained during the model validation, when the simulated data were fitted to empirical data, in particular, the simulated FC and the corresponding empirical FC. Here, the ICCs were calculated for the weights (correlation coefficients) of every *N(N-1)/2* undirected edges of the functional connectomes (empirical and simulated). The calculated *ICC* reflects the between-subject variance of these quantities relative to the total variance (between- and within-subject), and is given by the following expression (Liljequist, Elfving and Roaldsen, 2019): $ICC = \sigma^2_{subject}/(\sigma^2_{subject} + \sigma^2_{\varepsilon})$. Here, $\sigma^2_{subject}$ is the variance of the considered quantity (connectome edge weight) that is related to the variance among the subjects, and σ^2_{ε} is the residual variance induced by the different fMRI acquisitions. Such an implementation of the ICC has been recommended for the case when no convincing argument can be made that the residual noise contains additional consistent effects, and we wielded the equations proposed by (Liljequist, Elfving and Roaldsen, 2019) in order to calculate the ICC directly from the data.

4. Results

Here we present 3 studies (Domhof *et al.*, 2021; Popovych *et al.*, 2021; Domhof, Eickhoff and Popovych, 2022b) that considered different numbers of parcellations and investigated their impact on the empirical data and modeling results. We especially focus on the impact of parcellation granularity on

the modeling outcomes. Below we show that while some optimal granularity could be observed for some particular atlases and model fitting modalities, the general trend may indicate that the best model fit with the enhanced similarity between simulated and empirical data could be achieved for small number of brain parcels. The latter can account for the models' variability across brain atlases to a limited extent, and the other properties of the parcellations and their effects should be investigated for a better understanding of the modeling results.

4.1. Impact of atlas granularity on empirical and simulated data

Here we illustrate the impact of brain parcellations and their granularity on GoF values of the whole-brain dynamical models based on the phase and limit-cycles models for local dynamics, see Ref. (Popovych *et al.*, 2021) for more details. As mentioned above the brain parcellations were given by the Schaefer atlas (Schaefer *et al.*, 2018) of 100, 200, 400 and 600 cortical regions (S100, S200, S400 and S600), the Harvard-Oxford atlas (Desikan *et al.*, 2006) with the maximal probability thresholds at 0%, 25%, 35%, and 45% (HO96 0%, HO96 25%, HO96 35%, and HO96 45%) and the Shen atlas (Shen *et al.*, 2013) of 79, 156 and 232 cortical regions (Shen79, Shen156 and Shen232). The resting-state dynamics was simulated for 272 unrelated HCP (Van Essen *et al.*, 2013) subjects.

The impact of these parcellations on the quality of the functional model validation is illustrated in Figure 3A-D, where the simulated FC (sFC) was fitted to the empirical FC (eFC) such that the correlation between sFC and eFC was maximized by optimization of the model parameters. The distributions of the GoF values of the strongest correlation between sFC and eFC (denoted by Fit(sFC, eFC)) for individual subjects are depicted for the considered brain parcellations in Figure 3A and C. The impact of the parcellations is apparent when comparing the differences between Fit(sFC, eFC) for the Schaefer atlas (S100-S600, blue violins), the Harvard-Oxford atlas (HO96 0%-45%, yellow - dark red violins) and the Shen atlas (Shen79-Shen232, green violins) [Fig. 3A, C]. In the latter cases (HO96 and Shen) the both models demonstrate much higher fitting to the empirical data with respect to S100-S600 cases with up to 80% of the relative increase of Fit(sFC, eFC). The differences in the model fitting can also be observed between the parcellations of the same type, i.e., from the same atlas. In particular, the best fit for the Schaefer atlas was obtained for S200 case providing an optimal spatial scale, i.e., optimal granularity for this brain atlas (Figure 3A). However, the differences between Fit-values for different parcellations of the Schaefer atlas are small. For the other considered atlases Fit(sFC, eFC) monotonically decays when the threshold for HO96 atlas or the number of parcels for the Shen atlas increases [Figure 3A , C].

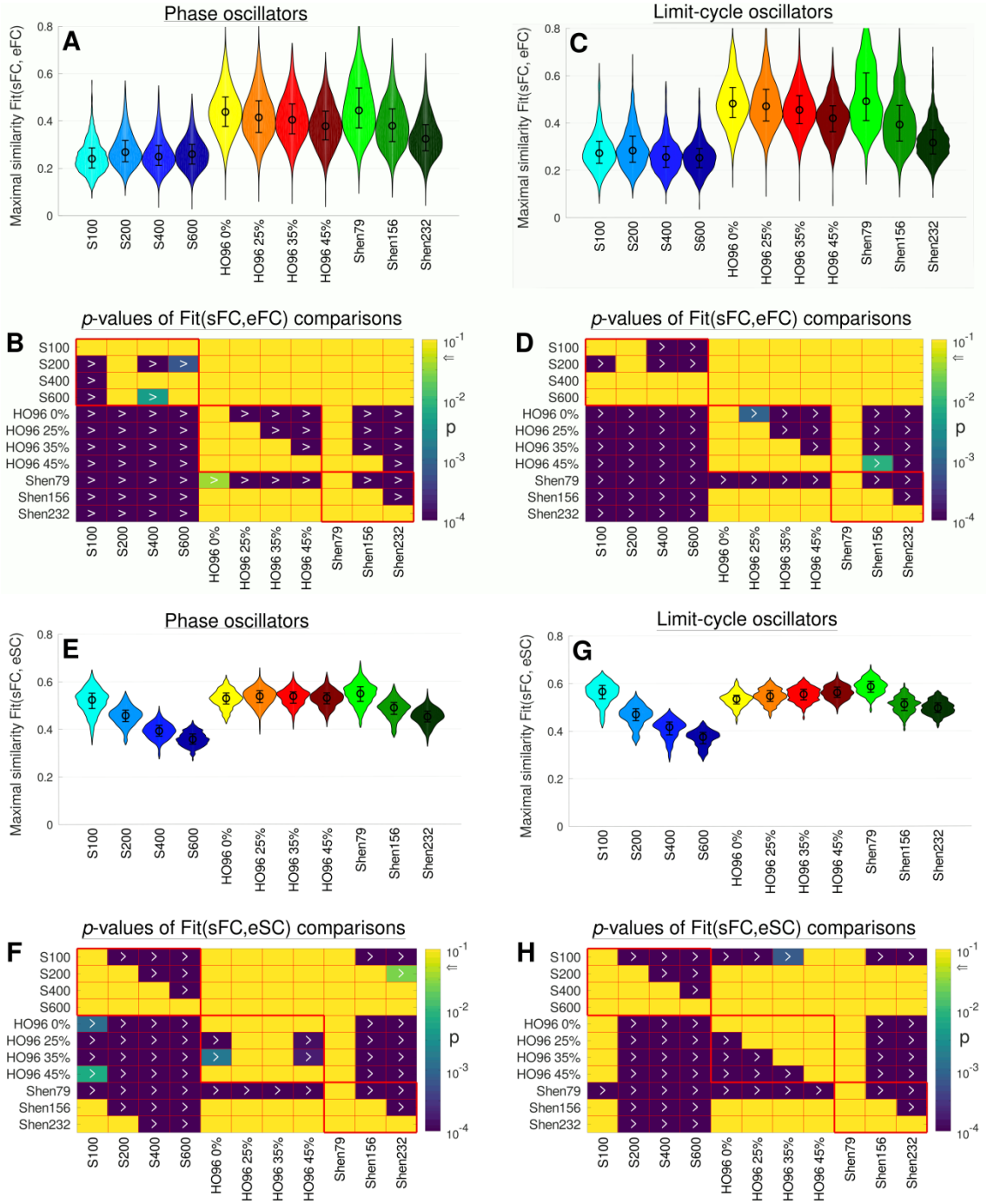

Figure 3. Results of (A-D) the functional and (E-H) structure-functional model fitting for (A, B, E, F) the phase model and (C, D, G, H) the limit-cycle model. (A, C, E, G) Distributions of the GoF values referring to the maximal similarity (correlation) between (A, C) sFC and eFC (Fit(sFC, eFC)) and (E, G) sFC and eSC (Fit(sFC, eSC)) as violin plots for the considered brain parcellations denoted on the horizontal axes as introduced in the text, where the medians and the interquartile ranges are also shown. (B, D, F, H) Outcomes of statistical comparisons, where the *p*-values (corrected for multiple comparisons) of the paired Wilcoxon signed-rank test of (B, D) Fit(sFC, eFC) and (F, H) Fit(sFC, eSC) values between the parcellations indicated on the axes are depicted by color in logarithmic scale (see color bar). The null hypothesis is rejected with $p < 0.05$ (indicated by arrow on the color bar) in favor of the alternative hypothesis Fit(row) > Fit(column) for parcellations in the row and column, respectively, where the corresponding cell is dark (small *p*-value) and contains the inequality sign ">".

Results of systematic statistical comparisons of Fit(sFC, eFC) between any two considered simulation conditions (11 parcellations) are illustrated in Figure 3B and D. Here, the *p*-values of the paired Wilcoxon signed-rank tests are depicted in color for comparisons between Fit-values of different parcellations.

The dark color (darker than yellow) at the intersection of a particular row and column (table cell) of the shown matrices indicates that the GoF values for the condition from the vertical axis Fit(row) are statistically larger (with $p < 0.05$ at least) than those of for the condition from the horizontal axis, Fit(column), accordingly. For example, the cells at the intersection of the row "S200" and columns "S100", "S400" and "S600" are dark implying $p < 0.05$ and marked by ">" (Figure 3B, D) implying Fit(S200) > Fit(S100) as well as Fit(S200) > Fit(S400) and Fit(S200) > Fit(S600). Based on these calculations, we also confirm that the quality of the model fitting is the best for the largest region sizes for the Harvard-Oxford atlas (see the row "HO96 0%" and its intersections wit the other "HO96"columns in Figure 3B and D) and decays for larger probability threshold, i.e., smaller regions for the Harvard-Oxford atlas. Similar is also true also for the Shen atlas, where smaller number of brain regions is beneficial for the model fitting to the empirical data [Figure 3B and D]. Shen79 provides the best fit for both models, whereas the lowest goodness-of-fit was obtained for S100 for the phase model and for S400 and S600 for the LC model, see the row "Shen79" and columns "S100", "S400" and "S600" in Figure 3B and D.

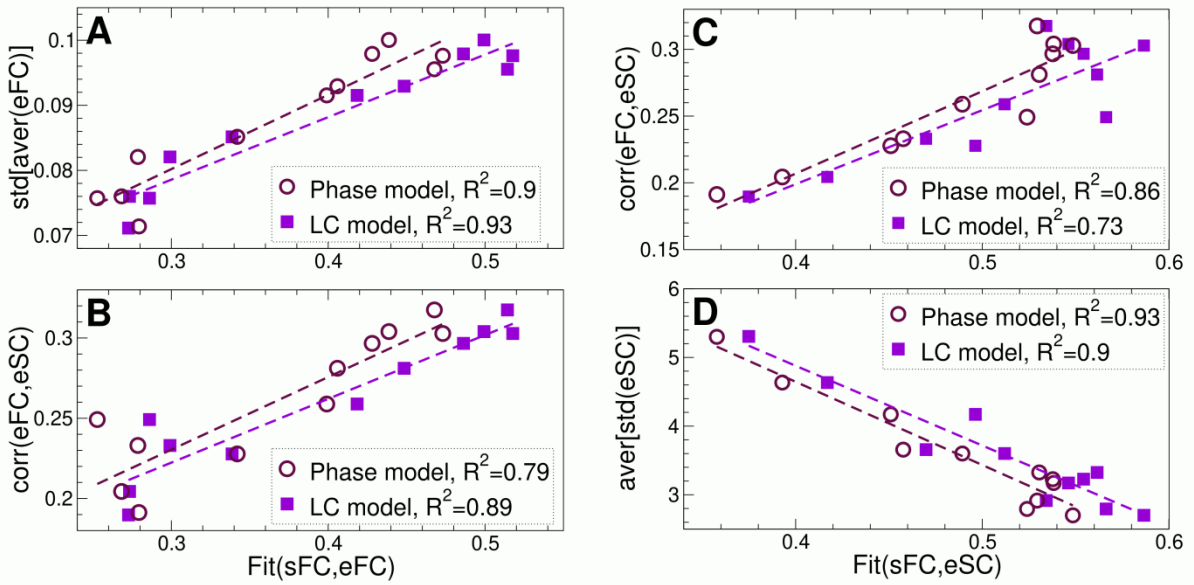

Figure 4. Correlation between the results of the model fitting (GoF) and data variables (data indices) at the group level. Scatter plots of the medians (across individual subjects) of some data variables versus (A, B) Fit(sFC, eFC) and (C, D) Fit(sFC, eSC) with the corresponding regression lines. Each plot symbol corresponds to one of the considered parcellations from Figure 3. The fractions of the explained variance (squared correlation) for both models of the phase and limit-cycle oscillators are indicated in the legends.

The situation is different for the structure-functional model validation illustrated in Figure 3E-H, where the simulated FC (sFC) was fitted to the empirical structural connectome (eSC) such that the correlation between sFC and eSC (streamline count) was maximized by optimization of the model parameters. The distributions of the GoF values of the best fitting between sFC and eSC (denoted by Fit(sFC, eSC)) are depicted in Figure 3E and G, and the results of statistical comparisons between different parcellations is shown in Figure 3F and H. In contrast to the functional model validation, the best structure-functional model fit takes place for the lowest number of parcels (coarsest granularity) S100 for the Schaefer atlas. For the Harvard-Oxford atlas, the best model fit takes place either for moderate (phase model, Figure 3E, F) or smallest (limit-cycle model, Figure 3G, H) region sizes (moderate and largest probability thresholds, respectively), which again differs from the results for the functional fitting (Figure 3A-D).

To understand the origin of the observed variation of the fitting results across brain parcellations, we suggested to evaluate how the Fit-values depend on a few data variables (or data indices) reflecting some statistical properties (Sec. 3.1) of the empirical data used for the model derivation and validation. We thus correlated the medians (calculated across all subject in the sample) of the Fit-values and the considered data variables across parcellations, and the results of the calculations are illustrated in Figure 4. Several data variables exhibit strong correspondence with the Fit-values for both models. However, only a few of them are significantly correlated with the GoF values. For the functional modal fitting, only two data indices *std*[*aver*(eFC)] and *corr*(eFC, eSC) significantly and strongly contribute to the inter-parcellation variance of Fit(sFC, eFC) at the group level for both models [Figure 4A, B], where the fraction of the explained variance can reach 93%. For the structure-functional model fitting, more data variables significantly correlate with the maximal similarity Fit(sFC, eSC), but only four of them fulfill this requirement for both models simultaneously: *corr*(eFC, eSC) that also contributes to Fit(sFC, eFC), as well as data variables *aver*[*std*(eSC)], *std*[*aver*(ePL)] and *aver*[*std*(ePL)] calculated from the structural connectome as given by eSC and ePL matrices. The former two data indices are illustrated in Figure 4C and D. Again, the fraction of the explained variance can reach 93% for the data index calculated from eSC (Figure 4C, D). Interestingly, the empirical structure-function relationship *corr*(eFC, eSC) positively correlates with the variations of GoF values for both considered model fitting modalities (Figure 4B-C). Therefore, if we are interested in finding the most appropriate brain parcellation and its granularity leading to the highest quality of the model validation, we may inspect the impact of the parcellations on this empirical data variable and search for the largest structure-function relationship.

4.2. Generalization for more models, parcellations and network properties

In this section we extend our consideration to more whole-brain models based on the coupled phase oscillators and neuronal mass models as well as to more brain parcellations listed in Table 1. The results of the model simulations performed for 200 HCP subjects were compared with a few graph-theoretical metrics of the empirical connectomes reflecting the impact of the parcellations on both empirical and simulated data, see Ref. (Domhof *et al.*, 2021) for more details. In this deliverable we focus on the impact of parcellation granularity on the empirical data (connectomes) used for the modeling and on the modeling results. The empirical BOLD signals and connectomes as well as simulation results of this study were published in three datasets on the EBRAINS platform and are ready for use by other researchers (Domhof, Eickhoff and Popovych, 2022a; Domhof *et al.*, 2022b, 2022a).

The results of the model validation for all brain atlases in Table 1 and the two considered whole-brain models of coupled phase oscillators and neural mass models are illustrated in Figure 5. For each combination of subject, parcellation, and model, the optimal values of the varied model parameters were found by maximizing the Pearson correlation between the empirical and simulated FC matrices, which provided the GoF values of the model illustrated in Figure 5A for both models. For varying parcellations we observed a high variability of the fitting results, implying that the extent of correspondence between simulated and empirical FC is strongly depended on the selected parcellation. Here, the MIST parcellation with 31 parcels, the Desikan-Killiany atlas, the von Economo-Koskinas atlas, and the AAL atlas yielded the highest goodness-of-fits independently of the model type (Figure 5A, atlas indices 1, 16, 17, and 18, respectively).

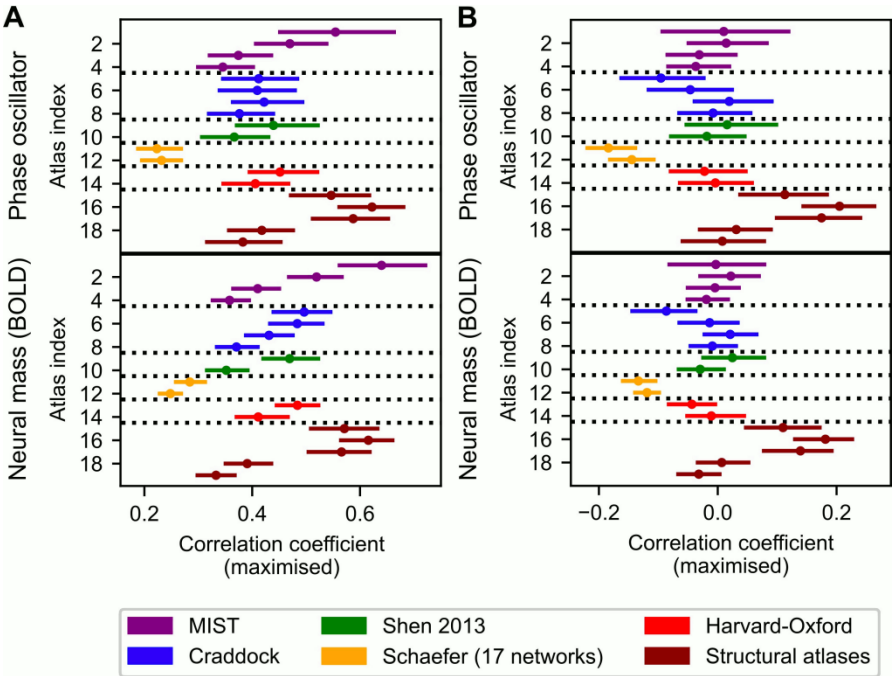

Figure 5. Maximized correlations (goodness-of-fit, GoF) between the empirical and simulated FC matrices for the brain parcellation schemes for the phase and neural mass models as indicated on the vertical axes. Dots and lines depict the medians and interquartile ranges across subjects, respectively. Table 1 contains the parcellation information corresponding to the atlas indices used in the plots, and the parcellation groups/atlases are indicated in legend. The difference between the plots (A) and (B) is that in plot (B) the effect of parcellation granularity (1/N, N – number of parcels) has been regressed out.

We also observed that the patterns of the GoF distributions versus parcellations were similar to each other for different models (Figure 5A, see also Fig. 3). To quantify the mentioned similarity, we considered the medians of the GoF values calculated over all subjects (Figure 5A, dots) and regress them across parcellations between the two models of the phase oscillators and the neural mass model. This resulted in a regression with a coefficient of determination of 0.88 suggesting a model-independent impact of a given brain parcellation on the (group-averaged) GoF values. To quantify the parcellation-induced influence on the GoF beyond the dependence on the parcellation granularity, the effect of the (inverted, 1/N, N – number of parcels) granularity was regressed out from the GoF values illustrated in Figure 5A. The residual GoF values exhibited variations across parcellations (Figure 5B) that had similar magnitudes as the original data, especially, between different brain atlases (parcellation algorithms), compare Figures 5A to 5B. In addition, the agreement between the models was further enhanced after regressing the parcellation granularity out, where the coefficient of determination between residual GoF values of different dynamical models increased up to 0.95 in Figure 5B.

We investigated the effect of the parcellation granularity on the graph-theoretical measures of empirical connectomes (eSC, ePL, eFC) and on the GoF values of the considered phase and neural mass models by calculating the Pearson correlation between their medians across subjects and the level of granularity, i.e., the inverse of the number of parcels (1/N) included in the parcellations. The calculation results are shown in Figure 6. We observed high and significant correlations between parcellation granularity and some of the considered network properties of the structural and functional connectomes, see the first column in Figure 6. In particular, the modularity and the clustering coefficient reflecting the segregation of the empirical eSC and eFC, and also the scale parameter of the eFC degree distribution are highly influenced by the parcellation granularity. The structure-function relationship $\rho_{SC,FC} = corr(eSC,eFC)$ is also governed by the number of regions to a large extent (high positive

correlation with 1/N), which is in agreement with the results of (Messe, 2019). However, most of the other network properties only weakly to moderately correlate with the parcellation granularity. We also found that the GoF values exhibited moderate and insignificant (after corrections for multiple comparisons) correlations with the parcellation granularity (Figure 6, table cells at the intersection of the first column of 1/N and the last rows for the phase and neural mass models), where the impact of granularity on the fitting results for the phase model is much smaller than that for the neural mass model.

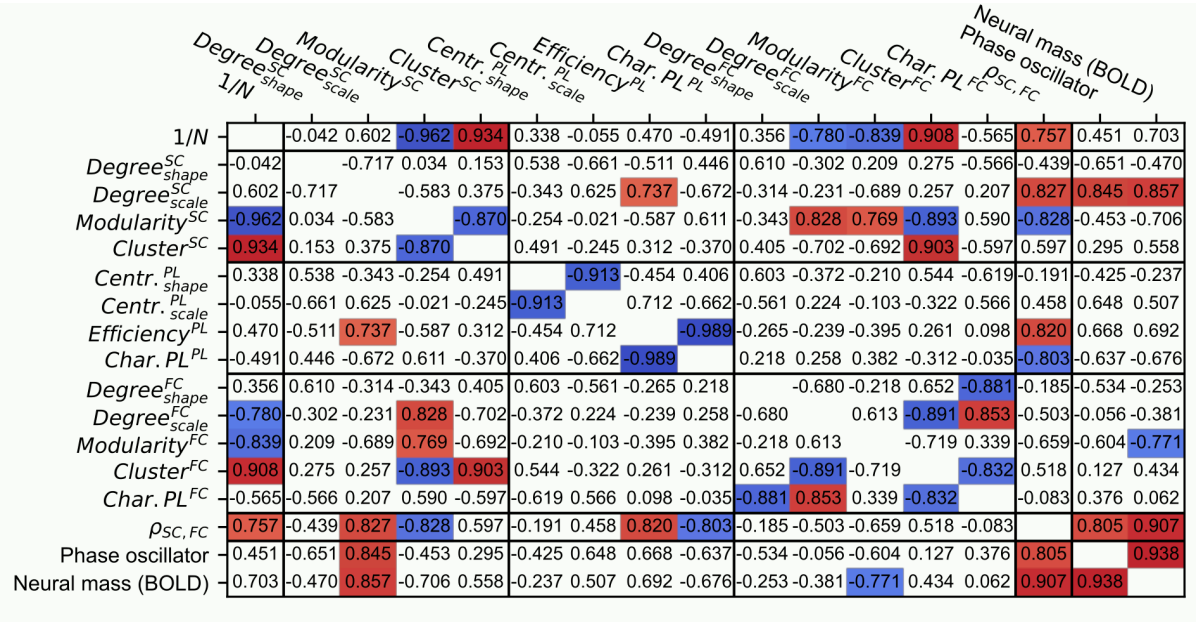

	1/N	Degree$^{SC}_{shape}$	Degree$^{SC}_{scale}$	Modularity^{SC}	Cluster^{SC}	Centr.$^{PL}_{shape}$	Centr.$^{PL}_{scale}$	Efficiency^{PL}	Char. PL^{PL}	Degree$^{FC}_{shape}$	Degree$^{FC}_{scale}$	Modularity^{FC}	Cluster^{FC}	Char. PL^{FC}	$\rho_{SC,FC}$	Phase oscillator	Neural mass (BOLD)
1/N		-0.042	0.602	-0.962	0.934	0.338	-0.055	0.470	-0.491	0.356	-0.780	-0.839	0.908	-0.565	0.757	0.451	0.703
Degree$^{SC}_{shape}$	-0.042		-0.717	0.034	0.153	0.538	-0.661	-0.511	0.446	0.610	-0.302	0.209	0.275	-0.566	-0.439	-0.651	-0.470
Degree$^{SC}_{scale}$	0.602	-0.717		-0.583	0.375	-0.343	0.625	0.737	-0.672	-0.314	-0.231	-0.689	0.257	0.207	0.827	0.845	0.857
Modularity^{SC}	-0.962	0.034	-0.583		-0.870	-0.254	-0.021	-0.587	0.611	-0.343	0.828	0.769	-0.893	0.590	-0.828	-0.453	-0.706
Cluster^{SC}	0.934	0.153	0.375	-0.870		0.491	-0.245	0.312	-0.370	0.405	-0.702	-0.692	0.903	-0.597	0.597	0.295	0.558
Centr.$^{PL}_{shape}$	0.338	0.538	-0.343	-0.254	0.491		-0.913	-0.454	0.406	0.603	-0.372	-0.210	0.544	-0.619	-0.191	-0.425	-0.237
Centr.$^{PL}_{scale}$	-0.055	-0.661	0.625	-0.021	-0.245	-0.913		0.712	-0.662	-0.561	0.224	-0.103	-0.322	0.566	0.458	0.648	0.507
Efficiency^{PL}	0.470	-0.511	0.737	-0.587	0.312	-0.454	0.712		-0.989	-0.265	-0.239	-0.395	0.261	0.098	0.820	0.668	0.692
Char. PL^{PL}	-0.491	0.446	-0.672	0.611	-0.370	0.406	-0.662	-0.989		0.218	0.258	0.382	-0.312	-0.035	-0.803	-0.637	-0.676
Degree$^{FC}_{shape}$	0.356	0.610	-0.314	-0.343	0.405	0.603	-0.561	-0.265	0.218		-0.680	-0.218	0.652	-0.881	-0.185	-0.534	-0.253
Degree$^{FC}_{scale}$	-0.780	-0.302	-0.231	0.828	-0.702	-0.372	0.224	-0.239	0.258	-0.680		0.613	-0.891	0.853	-0.503	-0.056	-0.381
Modularity^{FC}	-0.839	0.209	-0.689	0.769	-0.692	-0.210	-0.103	-0.395	0.382	-0.218	0.613		-0.719	0.339	-0.659	-0.604	-0.771
Cluster^{FC}	0.908	0.275	0.257	-0.893	0.903	0.544	-0.322	0.261	-0.312	0.652	-0.891	-0.719		-0.832	0.518	0.127	0.434
Char. PL^{FC}	-0.565	-0.566	0.207	0.590	-0.597	-0.619	0.566	0.098	-0.035	-0.881	0.853	0.339	-0.832		-0.083	0.376	0.062
$\rho_{SC,FC}$	0.757	-0.439	0.827	-0.828	0.597	-0.191	0.458	0.820	-0.803	-0.185	-0.503	-0.659	0.518	-0.083		0.805	0.907
Phase oscillator	0.451	-0.651	0.845	-0.453	0.295	-0.425	0.648	0.668	-0.637	-0.534	-0.056	-0.604	0.127	0.376	0.805		0.938
Neural mass (BOLD)	0.703	-0.470	0.857	-0.706	0.558	-0.237	0.507	0.692	-0.676	-0.253	-0.381	-0.771	0.434	0.062	0.907	0.938	

Figure 6. Cross-correlations among the level of granularity (1/N, N – number of parcels), the graph-theoretical measures of the empirical connectomes, i.e., network properties of the empirical eSC, ePL and eFC (see Ref. (Domhof *et al.*, 2021) for more details), the structure-function relationship $\rho_{SC,FC}$ = *corr*(eSC,eFC) as correlation between eSC and eFC, and the GoF values of the phase oscillator and the neural mass models to the empirical data as maximal correlation between sFC and eFC. The cross-correlation was calculated across parcellations between the median values over all subjects. Significant correlations are highlighted by colors (p<0.05, two-sided, Bonferroni corrected).

In conclusion, even though the granularity of a parcellation can greatly influence some of the network statistics extracted from the empirical data, the observed parcellation-induced deviations typically go beyond such a simple relationship, see also Ref. (Domhof *et al.*, 2021). The granularity influences the modeling results (GoF) to a limited extent, implying that the parcellation-induced variability cannot exclusively be explained by this quantity. Possible positive correlations between the level of granularity (1/N) and GoF values may indicate that the strongest correspondence between the simulated end empirical data can be achieved for parcellations with the coarsest granularity, i.e., small number of parcels. In more detail, the positive correlations across parcellations between GoF values and the empirical structure-function relationship ($\rho_{SC,FC}$ = *corr*(eSC,eFC)) (Figures 4 and 6) together with a monotonic decay of the latter, see Ref. (Messe, 2019) and Figure 6, supports the above claim. These results seem to be model-independent and hold for the considered phase, limit-cycle and neural mass models for local dynamics, which generalizes the observations reported in Sec. 4.1 and study (Popovych *et al.*, 2021).

4.3. Reliability and subject specificity of the modeling results

Given the enhanced variability of the modeling results discussed in the previous sections, comprehensive assessments of their reliability and the subject specificity as well their relation with the empirical data are necessary. We therefore addressed the test-retest reliability and subject specificity of the results of the model validation and compare them with those of the empirical connectomes across a wide variety of conditions for model derivation and employed parcellation. We demonstrate that the results of the model fitting may be more reliable and subject specific than the empirical data used for model validation. However, our results also show that this finding highly depends on the modeling conditions and brain parcellation.

The workflow of the performed investigations is schematically outlined in Sec. 3.2 (Figure 2), see also Ref. (Domhof, Eickhoff and Popovych, 2022b). We assessed the reliability and the subject specificity of the fits of the dynamical whole-brain models to the empirical FC. Here, we independently fitted simulated FC by optimizing free model parameters to different realizations of the empirical FC calculated from different acquisitions of the resting-state fMRI data of individual subjects. We therefore obtained a few realizations of the optimal model parameters and sFC for every subject, which allows for investigation of the intra-subject variability of the modeling results (Sec. 3.2).

We performed our simulations for 6 different dynamical whole-brain model implementations to study how the distinct facets of model personalization and model complexity affect the results. The influence of the model personalization was studied by considering multiple versions of coupled phase oscillators of the Kuramoto type (Kuramoto, 1984). In particular, the model could be constructed either on the basis of the grand-averaged or personalized empirical SC, and could be simulated using either group-averaged or subject-specific region-specific oscillation frequencies extracted from the empirical BOLD signals. Taken together, we considered the phase oscillators

(1) using averaged empirical SCs and averaged frequencies,
(2) using personalized empirical SCs and averaged frequencies,
(3) using averaged empirical SCs and personalized frequencies and
(4) using personalized empirical SCs and personalized frequencies.

The first and the last modeling conditions define the least and the most personalized models considered, respectively. The influence of model complexity was studied using three different models with a similar extent of personalization based on individualized empirical SC and PL matrices. We employed a fully linear model as the least complex model, the Kuramoto model simulated with the group-averaged frequency profiles (case (2) above) as a moderately complex model, and a Wilson-Cowan neural mass model which has the most complex model description and implementation among all models wielded in this study.

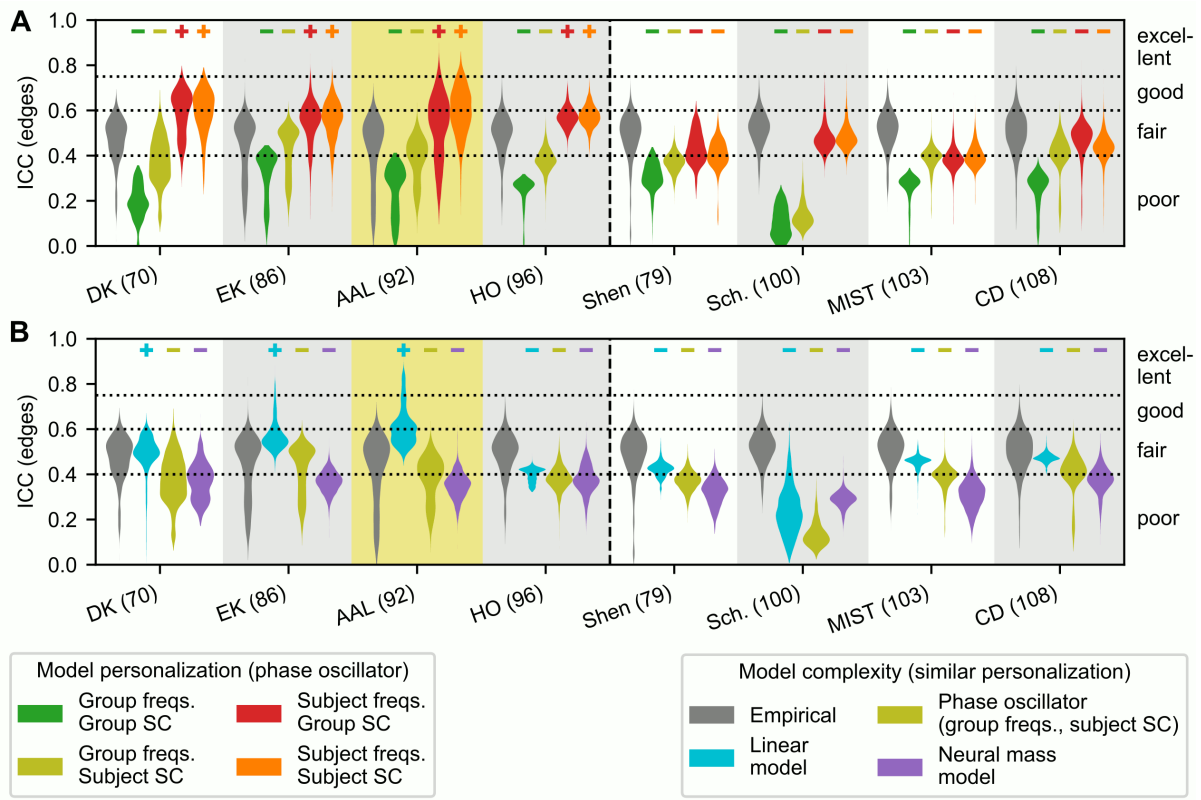

Figure 7. Reliability of modeling results for varying model personalization and complexity. The distributions of the ICC values (Sec. 3.2) of individual functional connections, edges of the empirical (gray) and simulated functional connectomes for all the atlases considered in this study for (A) the phase model of the same complexity with varying model personalization and (B) varying model complexity for a similar level of model personalization. The extent of the model personalization is given by the combinations of the subject-specific or group-averaged natural frequencies (freqs.) and SC and reflected by color as indicated in the legend. To vary the model complexity several models were considered, where the linear model (blue), the phase oscillator model (green) and the neural mass model (purple) corresponds to low, moderate and a high complexity, respectively. Plus and minus signs at the top of the plots signify significantly increased and decreased ICC distributions for the respective simulated FC with respect to the one for the empirical FC, correspondingly ($p < 0.05$, two-sided Wilcoxon paired signed-rank test, Bonferroni corrected). The labels ”poor”, ”fair”, ”good” and ”excellent” correspond to those proposed by (Cicchetti and Sparrow, 1981). The vertical dashed black lines separate the brain atlases constructed on the basis of structural data (left blocks) from those based on functional data (right blocks).

We first examined the reliability of the empirical and the simulated FC and calculated the ICC values (Sec. 3.2) of all empirical and simulated FC edges (individual functional connections between brain regions) and inspected their distributions. The ICCs of the empirical functional connections remained approximately at the same (”fair”) level across parcellations (Figure 7, gray). In contrast, the edge reliability of the simulated functional connectomes varied considerably across parcellations, and ranged from ”poor” to ”good”. These findings indicate that the reliability of the empirical FC is rather stable across parcellations, while that of the simulated FC is more sensitive to the utilized brain parcellations. We draw a specific attention to the positive influence of the model personalization on the reliability of the simulated connectome edges (Figure 7A): Simulating the phase oscillator model using subject-specific frequency profiles yielded higher reliability of sFC edges than using group-averaged frequency profiles practically irrespective of whether the group-averaged or personalized SC was used (Figure 7A, green vs. red and orange). The simulated FCs of the personalized phase oscillator model clearly exceeded the empirical FC in terms of edge reliability for all considered structurally-derived atlases irrespectively of the personalization of the empirical SC, and reached the ”good” level (Figure 7A, red

and orange). However, when considering the phase oscillator model simulated using group-averaged frequencies, the simulated FCs were also fitted with higher reliability when the personalized instead of the group-averaged SCs were used for model construction (Figure 7A, dark vs. light green). Hence, model personalization appears to promote the reliability of the model fit to the empirical data.

More complex models seemed to yield a reliability of the simulated FC edges that was less variant across parcellations, and a higher model complexity was not immediately more reliable at the same level of model personalization (Figure 7B, violent violins). On the other hand, the reliability of the simulated FC generated by the simplest linear model varied considerably across parcellations, can be higher than that for the non-linear models in many cases, and significantly exceeded that of the empirical FC for the Desikan-Killiany, von Economo-Koskinas and AAL atlases (Figure 7B, blue violins). The results of this investigation confirmed that an enhanced model complexity did not exert a positive influence on the reliability of the simulated FC, which was consistent across parcellations.

Several modeling conditions yielded simulated FCs with edges' reliability being lower than for the empirical FC (Figure 7). We therefore investigated whether the whole connectivity patterns of the simulated FCs were nevertheless similar given that they were fitted to different empirical FCs of the same subject. For this purpose, we evaluated the within-subject, single-modal connectome correlations (Figure 2). A considerable number of the modeling conditions and subjects yielded simulated FC matrices that had strongly diverging connectivity motifs, which is reflected by low intra-subject correlations between simulated FCs compared to the empirical FCs (Figure 8A-B, minus signs on top of the plots). In particular, increased model complexity led to more dissimilar within-subject simulated FCs for most parcellations (Figure 8B, violin distributions). Hence, the fit of the model to the empirical data could on average enhance the within-subject variability of the simulated FC as compared to empirical FC depending on the particular combination of model implementation and parcellation (Figure 4A-B, minus signs on top of the plots). Nevertheless, for most considered modeling conditions, we observed that the within-subject simulated FC matrices had connectivity patterns that were significantly more similar to one another than those of the empirical FC (Figure 8A-B, plus signs on top of the plots).

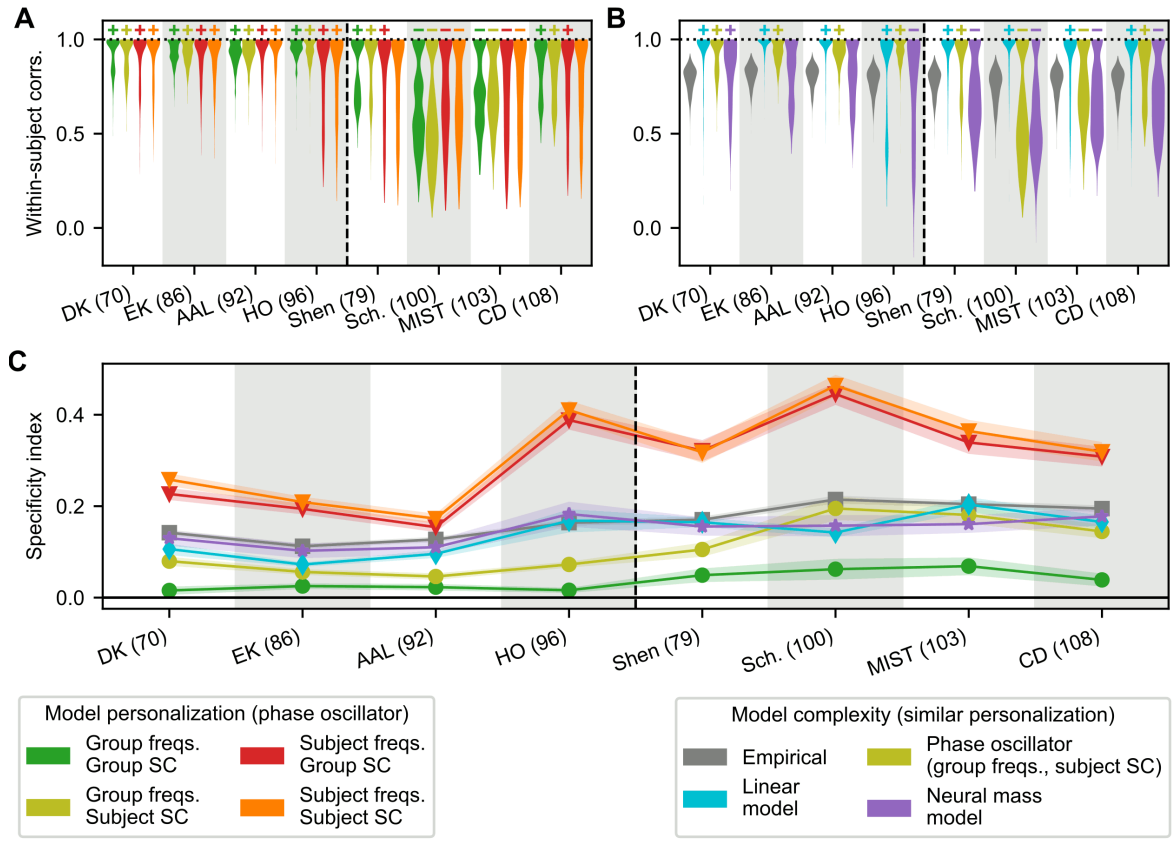

Figure 8. Impact of the brain atlas, model personalization and model complexity on the reliability and subject specificity of the connectivity patterns of the empirical (gray) and simulated FC. (A-B) Distributions of the within-subject, single-modal correlations (corrs.) as a reliability measure of the empirical and simulated FC patterns for the various parcellations considered in this study (indicated on the horizontal axes, see Sec 3.2) and for varying levels of (A) model personalization and (B) model complexity. Plus and minus signs at the top of the plots indicate significantly increased and decreased within-subject correlation distributions for the respective simulated FC with respect to the one for the empirical FC (gray; panel B), respectively ($p < 0.05$, two-sided Wilcoxon paired signed-rank test, Bonferroni corrected). (C) Specificity indices (Sec. 3.2) calculated from the single-modal correlations of the empirical FC and the simulated FC for varied model personalization and compexity. The symbols and shaded areas mark the medians and the (Bonferroni corrected) 95% confidence intervals across bootstrapped specificity index estimations, respectively. The extent of model personalization as given by the combinations of the subject-specific or group-averaged natural frequencies (freqs.) and SC is indicated in the legend shown in the lower left corner of the plot. Analogously, the level of model complexity as reflected by the linear (least complex), phase oscillator (moderately complex) and neural mass (most complex) models with similar personalization levels is indicated in the legend shown in the lower right corner. The vertical dashed black lines separate the brain atlases constructed on the basis of structural data (left blocks) from those based on functional data (right blocks).

We also calculated the specificity indices (Sec. 3.2) to determine the gain of the within- relative to the between-subject FC correlations. We observed that enhanced model personalization induced a clear increase in the specificity index that could exceed that of the empirical FC (Figure 8C). On the other hand, the least personalized model with the averaged frequencies and SC exhibited a very low subject specificity (Figure 8C, dark green) at a relatively high reliability of connectivity patterns as given by the intra-subject correlation of the simulated connectomes (Figure 8A, dark green). Conversely, varying the model complexity did not result in differences of the specificity indices that were consistent across parcellations (Figure 8C, blue, light green and purple). Hence, model personalization, but not model complexity had a positive effect on subject specificity measure (specificity index) that was consistent across parcellations.

In summary, most of the model implementations yielded within-subject correlations of the simulated FC that were significantly enhanced relative to the empirical FC. However, these significant enhancements actually reflected a general increase in both the within- and between-subject FC correlations such that the specificity index remained comparable with that of the empirical data. This is in particular true for the linear and non-linear models with a low and moderate extent of personalization (Figure 8). Only an enhanced model personalization can lead to much improvement of the subject specificity and also reliability of the simulated FC as a modeling result (Figures 7 and 8). Interestingly, the enhanced subject specificity of simulated FC is more pronounced for the functionally-derived brain parcellations (Figure 8C), while the ICC edges' reliability and the within-subject similarity of FC patterns, that can also be considered as a kind of reliability, are more enhanced for the structurally-derived parcellations (Figures. 7A and 8A).

5. Conclusion

We evaluated the impact of brain parcellations used for the calculation of empirical structural and functional connectomes on the modeling results of the whole-brain dynamical models that utilized the empirical neuroimaging data for their derivation and validation. We in particular focused on the parcellation granularity (number of brain regions) and showed that it is difficult to find any particular optimal parcellation granularity. One may observe some optimal granularity for some individual brain atlases, like 200 parcels for the Schaefer atlas for the functional model fitting or intermediate region size for a moderate maximal probability threshold of the Harvard-Oxford atlas for the structure-functional model fitting (Figure 3). However, the general tendency might be that a coarser granularity (less parcels) can lead to a better model fit to empirical data. This also agrees with the behavior of the empirical structure-function relationship that can well explain the variability of the GoF values across parcellations at the group level. The level of granularity (1/N, N – number of parcels) was found to positively correlate with GoF values. However, it can explain the model variability to a limited extent, and the inter-parcellation variability of the modeling results can go much beyond the number of regions in the brain parcellations. Here, the parcellation method may play a role.

Given the enhanced variability of the modeling results across different brain atlases, we therefore performed a systematic assessments of the reliability and the subject specificity of the modeling results and their relation to the empirical data for a set of brain parcellations with similar granularity, but representing different families of brain atlases derived from functional and structural brain properties. We found that the atlas families (functionally-based or structurally-based) may have different impact on the reliability and subject specificity of the modeling results, and that the model personalization rather than model complexity is important for the reliability and specificity of the modeling results. The reported findings make our study relevant for application of personalized models, especially, given the current focus on the involvement of dynamical whole-brain models in clinical investigations, for example, in the framework of personalized medicine. Based on our results we also suggest to verify the obtained modeling outcomes with respect to their reliability and specificity and involve a few brain parcellations in the analysis to confirm the derived conclusions for different parcellations.

6. References

Amico, E. and Goni, J. (2018) 'The quest for identifiability in human functional connectomes', Sci. Rep., 8, p. 8254. Available at: https://doi.org/10.1038/s41598-018-25089-1.

Arslan, S. et al. (2018) 'Human brain mapping: A systematic comparison of parcellation methods for the human cerebral cortex', Neuroimage, 170, pp. 5–30. Available at: https://doi.org/10.1016/j.neuroimage.2017.04.014.

Cicchetti, D.V. and Sparrow, S.A. (1981) 'Developing Criteria For Establishing Interrater Reliability of Specific Items - Applications To Assessment of Adaptive-behavior', Am. J. Ment. Defic., 86(2), pp. 127–137.

Desikan, R.S. et al. (2006) 'An automated labeling system for subdividing the human cerebral cortex on MRI scans into gyral based regions of interest', Neuroimage, 31(3), pp. 968–980. Available at: https://doi.org/10.1016/j.neuroimage.2006.01.021.

Domhof, J.W.M. et al. (2020) 'Evaluation of cross-model atlas-based compression for machine learning', VirtualBrainCloud, ID 82642, H2020, Deliverable 3.9.

Domhof, J.W.M. et al. (2021) 'Parcellation-induced variation of empirical and simulated brain connectomes at group and subject levels', Network Neuroscience, 5(3), pp. 798–830. Available at: https://doi.org/10.1162/netn_a_00202.

Domhof, J.W.M. et al. (2022a) 'Parcellation-based resting-state blood-oxygen-level-dependent (BOLD) signals of a healthy cohort (v1.0) [Data set]', EBRAINS [Preprint]. Available at: https://doi.org/10.25493/F9DP-WCQ.

Domhof, J.W.M. et al. (2022b) 'Parcellation-based structural and resting-state functional brain connectomes of a healthy cohort (v1.1) [Data set]', EBRAINS [Preprint]. Available at: https://doi.org/10.25493/NVS8-XS5.

Domhof, J.W.M., Eickhoff, S.B. and Popovych, O.V. (2022a) 'Parcellation-based functional connectivity simulated by personalized whole-brain dynamical models (1.0) [Data set]', EBRAINS [Preprint]. Available at: https://doi.org/10.25493/CBE0-EQV.

Domhof, J.W.M., Eickhoff, S.B. and Popovych, O.V. (2022b) 'Reliability and subject specificity of personalized whole-brain dynamical models', NeuroImage, 257, p. 119321. Available at: https://doi.org/10.1016/j.neuroimage.2022.119321.

Eickhoff, S.B., Constable, R.T. and Yeo, B.T.T. (2018) 'Topographic organization of the cerebral cortex and brain cartography', Neuroimage, 170, pp. 332–347. Available at: https://doi.org/10.1016/j.neuroimage.2017.02.018.

Eickhoff, S.B., Yeo, B.T.T. and Genon, S. (2018) 'Imaging-based parcellations of the human brain', Nat. Rev. Neurosci., 19(11), pp. 672–686. Available at: https://doi.org/10.1038/s41583-018-0071-7.

Ghosh, A. et al. (2008) 'Noise during Rest Enables the Exploration of the Brain's Dynamic Repertoire', PLoS Comput. Biol., 4(10), p. e1000196. Available at: https://doi.org/10.1371/journal.pcbi.1000196.

Honey, C.J. et al. (2009) 'Predicting human resting-state functional connectivity from structural connectivity', Proc. Natl. Acad. Sci. U. S. A., 106(6), pp. 2035–2040. Available at: https://doi.org/10.1073/pnas.0811168106.

Jülich Supercomputing Centre (2021) 'JURECA: Data Centric and Booster Modules implementing the Modular Supercomputing Architecture at Jülich Supercomputing Centre', Journal of large-scale research facilities, 7, p. A182. Available at: https://doi.org/10.17815/jlsrf-7-182.

Jung, K. et al. (2022) 'Whole-brain dynamical modelling for classification of Parkinson's disease', Brain Communications, 5(1), p. fcac331. Available at: https://doi.org/10.1093/braincomms/fcac331.

Jung, K., Eickhoff, S.B. and Popovych, O.V. (2021) 'Tractography density affects whole-brain structural architecture and resting-state dynamical modeling', NeuroImage, 237, p. 118176. Available at: https://doi.org/10.1016/j.neuroimage.2021.118176.

Kuramoto, Y. (1984) Chemical oscillations, waves, and turbulence. Berlin: Springer.

Liljequist, D., Elfving, B. and Roaldsen, K.S. (2019) 'Intraclass correlation - A discussion and demonstration of basic features', Plos One, 14(7), p. e0219854. Available at: https://doi.org/10.1371/journal.pone.0219854.

Messe, A. (2019) 'Parcellation influence on the connectivity-based structure-function relationship in the human brain', Hum. Brain Mapp., pp. 1–14. Available at: https://doi.org/10.1002/hbm.24866.

Park, H.J. and Friston, K.J. (2013) 'Structural and Functional Brain Networks: From Connections to Cognition', Science, 342(6158), p. 1238411. Available at: https://doi.org/10.1126/science.1238411.

Pervaiz, U. et al. (2020) 'Optimising network modelling methods for fMRI', NeuroImage, 211, p. 116604. Available at: https://doi.org/10.1016/j.neuroimage.2020.116604.

Popovych, O. and Eickhoff, S. (2021) 'Framework for multi-modal integrated annotations established and in use', VirtualBrainCloud, ID 82642, H2020, Deliverable 3.10.

Popovych, O.V. et al. (2019) 'What Can Computational Models Contribute to Neuroimaging Data Analytics?', Front. Syst. Neurosci., 12, p. 68. Available at: https://doi.org/10.3389/fnsys.2018.00068.

Popovych, O.V. et al. (2021) 'Inter-subject and inter-parcellation variability of resting-state whole-brain dynamical modeling', NeuroImage, 236, p. 118201. Available at: https://doi.org/10.1016/j.neuroimage.2021.118201.

Proix, T. et al. (2016) 'How do parcellation size and short-range connectivity affect dynamics in large-scale brain network models?', Neuroimage, 142, pp. 135–149. Available at: https://doi.org/10.1016/j.neuroimage.2016.06.016.

Rubinov, M. and Sporns, O. (2010) 'Complex network measures of brain connectivity: Uses and interpretations', Neuroimage, 52(3), pp. 1059–1069. Available at: https://doi.org/10.1016/j.neuroimage.2009.10.003.

Schaefer, A. et al. (2018) 'Local-Global Parcellation of the Human Cerebral Cortex from Intrinsic Functional Connectivity MRI', Cereb. Cortex, 28(9), pp. 3095–3114. Available at: https://doi.org/10.1093/cercor/bhx179.

Shen, X. et al. (2013) 'Groupwise whole-brain parcellation from resting-state fMRI data for network node identification', Neuroimage, 82, pp. 403–415. Available at: https://doi.org/10.1016/j.neuroimage.2013.05.081.

Sporns, O., Tononi, G. and Kotter, R. (2005) 'The human connectome: A structural description of the human brain', PLoS Comput. Biol., 1(4), p. e42. Available at: https://doi.org/10.1371/journal.pcbi.0010042.

Thirion, B. et al. (2014) 'Which fMRI clustering gives good brain parcellations?', Front. Neurosci., 8, p. 167. Available at: https://doi.org/10.3389/fnins.2014.00167.

Van Essen, D.C. et al. (2013) 'The WU-Minn Human Connectome Project: An overview', Neuroimage, 80, pp. 62–79. Available at: https://doi.org/10.1016/j.neuroimage.2013.05.041.

Zalesky, A. et al. (2010) 'Whole-brain anatomical networks: Does the choice of nodes matter?', Neuroimage, 50(3), pp. 970–983. Available at: https://doi.org/10.1016/j.neuroimage.2009.12.027.

Zimmermann, J. et al. (2019) 'Subject specificity of the correlation between large-scale structural and functional connectivity', Network Neuroscience, 3(1), pp. 90–106. Available at: https://doi.org/10.1162/netn_a_00055.